Solvothermal One-Pot Synthesis of a New Family of Chiral [Fe$_4$O$_4$]-Cubane Clusters with Redox Active Cores

Marco Seifried [1,*], Frieda M. Kapsamer [1], Michael Reissner [2], Jan M. Welch [3], Gerald Giester [4], Danny Müller [1] and Peter Weinberger [1,*]

1   Institute of Applied Synthetic Chemistry, TU Wien, Getreidemarkt 9/163-01-3, 1060 Vienna, Austria
2   Institute of Solid State Physics, TU Wien, Wiedner Hauptstraße 8-10/050, 1040 Vienna, Austria
3   Center for Labelling and Isotope Production, TRIGA Center Atominstitut, TU Wien, Stadionallee 2,
     1020 Vienna, Austria
4   Department of Mineralogy and Crystallography, University of Vienna, Josef-Holaubek-Platz 2 (UZA 2),
     1090 Vienna, Austria
*   Correspondence: marco.seifried@tuwien.ac.at (M.S.); peter.e163.weinberger@tuwien.ac.at (P.W.)

Abstract: The two achiral ligands tris(1-methyl-*1H*-imidazol-2-yl)methanol ((mim)$_3$COH) and bis(1-methyl-*1H*-imidazol-2-yl)(3-methylpyridin-2-yl)methanol ((mim)$_2$(mpy)COH) form on reaction with Fe(BF$_4$)$_2$·6H$_2$O, the octahedral low-spin complexes [Fe((mim)$_3$COH)$_2$](BF$_4$)$_2$·MeCN (**1**) and [Fe((mim)$_2$(mpy)COH)$_2$](BF$_4$)$_2$·0.5MeCN (**2**). Both octahedral complexes immediately rearrange to the chiral [Fe$_4$O$_4$]-cubane clusters [Fe$_4$(mim)$_3$CO)$_4$](BF$_4$)$_4$ (**3**) and [Fe$_4$(mim)$_3$CO)$_4$](BF$_4$)$_4$·CHCl$_3$ (**4**), whereas the highly symmetrical **3** crystallizes as racemate, **4** resolves based on the asymmetry introduced by the 2-methylpyridine moiety and crystallizes as an enantiomerically pure sample. Both clusters feature redox active [Fe$_4$O$_4$]-cubane cores with up to four individual accessible states, which directs towards a potential application as electron-shuttle.

Keywords: [Fe$_4$O$_4$]-cubane core cluster; magnetic properties; electrochemistry; imidazoles

1. Introduction

Tuning the ligand field strength in octahedral azole Fe(II) complexes to obtain spin-state switchable materials requires a carefully weighted equilibrium between sterics [1] and electronics [2]. Especially for multidentate azole systems, the ligands' strain can be highly dominant, affecting the geometry around the central Fe(II) atom. A comprehensive review on this phenomenon was published by M. Halcrow [3] using the example of Fe(II) complexes of (substituted) 2,6-di(pyrazol-1-yl)pyridines. Due to the rigid ligands' backbone, the corresponding Fe(II) complexes are affected by a—for Fe(II) unusual—Jahn Teller distortion, which limits the occurrence of spin crossover to a narrow range of angles between the ligands that still allow both the occurrence of the low-spin and high-spin state.

Multi-dentate azole ligands are, in general, a valuable platform for studies on structure–property relationships in spin crossover materials, as the final complex geometry is consistently predictable based on the systems' parent–meaning unfunctionalized ligand. To avoid the steric challenges inherent to a stiff ligand system such as, e.g., the 2,6-di(pyrazol-1-yl)pyridine, a more flexible design was found in the tris(2-imidazolyl)carbinol reported in 1978 by Breslow et al. as a model for the zinc-binding site of the carbonic anhydrase and alkaline phosphatase [4]. Based on their studies, the reported tripodal ligand system was used in further coordination studies with more transition metals such as metallo-enzyme proxies [5,6].

The tris(azole)methanol provides access to a vast library of tripodal azole ligands, providing huge versatility at the cost of undergrad synthetic protocols. Synthetic modification is easily executed by reaction on the -COH site, as well as depending on the used azoles for the ligands' synthesis in direct proximity to the coordinated Fe(II). The azoles

(most of them commercially available at low cost in a multi-gram scale) especially allow for variation of ring size, number of available coordination sites in the ring, and substituents for adjusting the ligands' cone angle. This enables the systematic investigation of the azoles' impact on the magnetic and spectroscopic properties of their coordination compounds.

Besides their ability to form hexacoordinated transition metal complexes, imidazoles also tend to stabilize $[Me_4-\mu_3-O_4]$ cubane-type clusters. With iron, multiple synthetic iron-oxo clusters with the Fe_4O_4 cubane motif have been prepared to study the feasibility of their occurrence in nature and compare their behavior with the known iron-sulfur proteins [7–19]. Many single valent cores, mostly with the Fe(II) configuration, or mixed valence compounds with mixtures of Fe(II/III) centers have been prepared, most of them either with carboxylate ligands or as part of large polynuclear complexes. So far, no tetranuclear Fe_4O_4 clusters employing tridentate ligands without iron atoms outside the core cubane structure have been reported.

Interested in the impact that the variation of the azoles in the tripodal ligand system would have on the Fe(II) spin crossover properties, as well as in these ligands' $[Fe_4O_4]$ clusters that could be formed, Breslow's tris(2-imidazolyl)carbinol (II) ligand was N-methylated to avoid the interaction of the basic NH site with the Fe(II) during coordination. For comparison, tris(1-methyl-*1H*-imidazol-2-yl)methanol $((mim)_3COH)$ and bis(1-methyl-*1H*-imidazol-2-yl)(3-methylpyridin-2-yl)methanol $((mim)_2(mpy)COH)$, having one 2-methylimidazole exchanged for a notably larger 2-methylpyridine, were chosen.

2. Results and Discussion

The reaction of $(mim)_3COH$ and $(mim)_2(mpy)COH$ with $Fe(BF_4)_2 \cdot 6H_2O$ under inert atmosphere resulted at room-temperature in the formation of the homoleptic mononuclear complexes $[Fe((mim)_3COH)_2](BF_4)_2 \cdot MeCN$ (**1**) and $[Fe((mim)_2(mpy)COH)_2](BF_4)_2 \cdot 0.5\,MeCN$ (**2**) in a low-spin configuration. Gentle heating of the reaction mixture to 40 °C resulted in the initially colorless reaction mixture of $((mim)_3COH)$ turning to a dark blue color over time. Further investigation of this observation resulted in the development of a solvothermal protocol, allowing for the isolation of two iron-oxo clusters with a $[Fe_4O_4]$-cubane-like core: $[Fe_4((mim)_3CO)_4](BF_4)_4$ (**3**) and $[Fe_4((mim)_2(mpy)CO)_4](BF_4)_4 \cdot CHCl_3$ (**4**).

The cluster compounds could be prepared either in situ from pure ligand and iron precursor or as a two-step reaction after isolation of the mononuclear complexes.

Following the dark blue color during the formation of **3**, a side reaction could be identified, as, under solvothermal conditions, the $(mim)_3COH$ ligand was found to be prone to the elimination of one imidazole moiety. The resulting bis(imidazolyl)ketone ligand formed with the Fe(II) in the solution the previously reported dark blue $[Fe((Me-bik)_3](BF_4)_2$ (**5**) [20]. Figure 1 depicts the entire reaction scheme.

The elimination of the imidazole from $(mim)_3COH$ at elevated temperatures is promoted by the ligands' basicity. To shift the equilibrium, the reaction was investigated under the addition of three equivalents of N-methylimidazole, as well in a slightly acidic environment. However, in all cases, the elimination could not be prevented. For $(mim)_2(mpy)COH$, no elimination reaction was evidenced, which seems to be a combination of the increased steric bulk due to the 2-methylpyridine moiety, as well as to the slightly lower basicity.

2.1. Structural Characterization

$[Fe((mim)_3COH)_2](BF_4)_2 \cdot MeCN$ (**1**) crystallizes as a stable acetonitrile solvate (Figure 2a) in the monoclinic space group *C2/c*, the Fe(II)-core located on the Wyckoff-position 4*a* ($\frac{1}{2}$, $\frac{1}{2}$, $\frac{1}{2}$). The Fe-N bond lengths vary between 1.902 and 1.924 Å, which is in good agreement with literature for Fe(II)–azole complexes in the low-spin state. The angular deviation parameter, defined as the sum of the deviation from an ideal octahedral angle of 90° of the 12 cis angles in the coordination sphere, is calculated with $\Sigma = 37.9°$ [21]. The continuous-shape measures [22] against an ideal octahedron to give a shape-deviation parameter $S_O = 0.13$, which aligns with a near-ideal octahedral geometry of the complex cation. On a supramolecular level, **1** forms infinite chains parallel to the

c-axis, the individual [Fe((mim)$_3$COH)$_2$]$^{2+}$-cations associated to each other by the formation of stabilizing hydrogen bonds between the ligands' OH-groups (Figure 2b). The strain introduced through the hydrogen bonds causes a twist of the [Fe((mim)$_3$COH)$_2$]$^{2+}$-cations by 28.29° towards each other, giving rise to a characteristic zig-zag orientation of the chains.
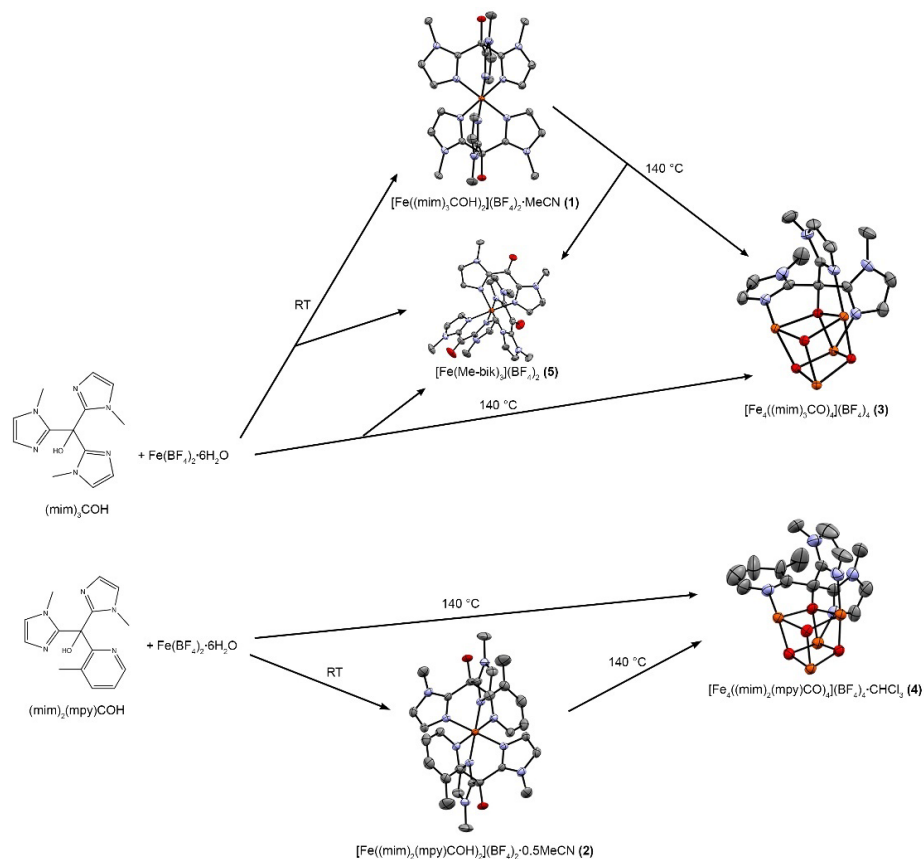

Figure 1. Reaction scheme for the cluster formation, with hydrogens, anions, and solvates omitted. (**top**) (mim)$_3$COH coordinates Fe(BF$_4$)$_2$·6H$_2$O, resulting in the octahedral complex **1** and the rearranged elimination product **5**. Solvothermal reaction of ligand and Fe(II) or solvothermal treatment of **1** yield [Fe$_4$O$_4$]-cluster **3** with **5** as a competing path. (**bottom**) (mim)$_2$(mpy)COH coordinates Fe(BF$_4$)$_2$·6H$_2$O resulting in the octahedral complex **2**. Solvothermal reaction of ligand and Fe(II) or solvothermal treatment of **2** yields [Fe$_4$O$_4$]-cluster **4**.

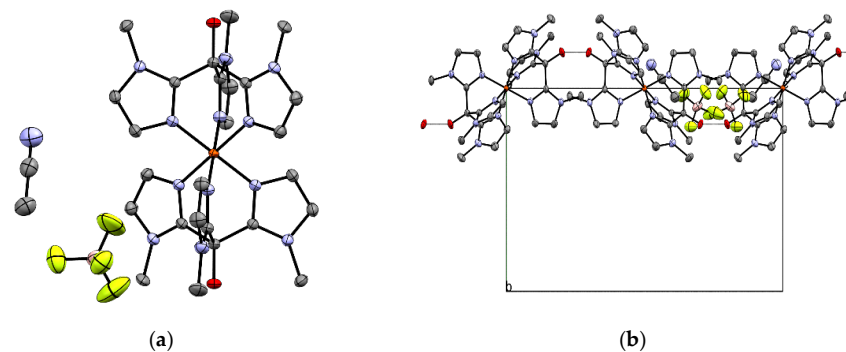

Figure 2. (**a**) Molecular structure of [Fe((mim)$_3$COH)$_2$](BF$_4$)$_2$·MeCN (**1**). (**b**) Zig-zag chains of **1** parallel to the *z*-axis, stabilized through intramolecular hydrogen bonds between the ligands' OH-groups.

[Fe((mim)$_2$(mpy)COH)$_2$](BF$_4$)$_2$·0.5MeCN (**2**) crystallizes as 0.5 MeCN solvate in the triclinic space group $P\bar{1}$ with two molecules of **2** per unit cell. The Fe-atoms are located at the Wyckoff positions 1*h* ($\frac{1}{2}$, $\frac{1}{2}$, $\frac{1}{2}$) and 1*c* (0, $\frac{1}{2}$,1; 1, $\frac{1}{2}$, 1; 1, $\frac{1}{2}$, 0; 1, $\frac{1}{2}$, 1). Moreover, for **2**, the Fe-N bond lengths are typical for Fe(II) low-spin complexes with 1.944–1.983 Å. Only the Fe-N bonds to the pyridine-N are slightly longer, with 2.011 Å (Fe1) and 2.014 Å (Fe2) (Figure 3a). For both Fe(II) atoms, the angular deviation parameter results $\Sigma = 30.4°$, and the shape-deviation parameter of $S_O = 0.14$ is also for **2**, which is in alignment with a near-ideal octahedral geometry.
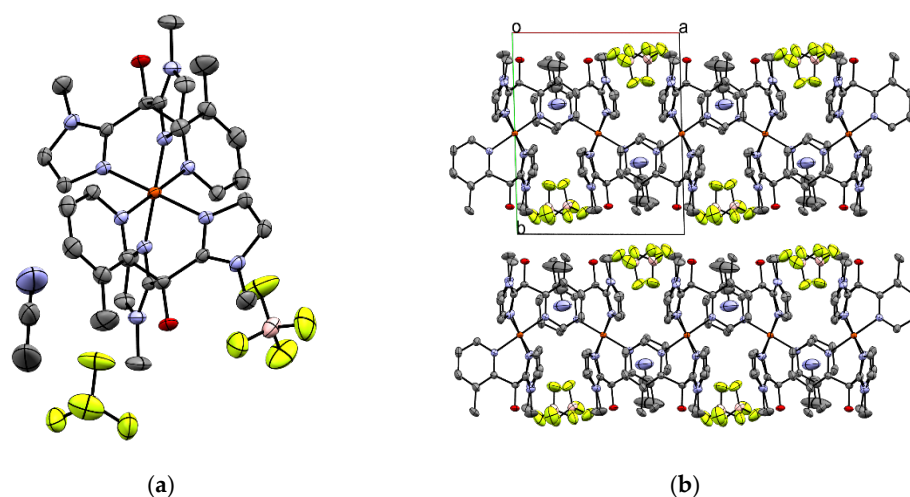

(a)   **(b)**

Figure 3. (**a**) Molecular structure of [Fe((mim)$_2$(mpy)COH)$_2$](BF$_4$)$_2$·0.5MeCN (**2**). (**b**) Stacking of infinite chains of interacting [Fe((mim)$_2$(mpy)COH)$_2$]$^{2+}$ molecules along the *b*-axis with a clear view on the nitrilic nitrogen interacting with the pyridine in the ligand through n $\rightarrow$ π^*_{Ar} interactions.

On a supramolecular level, **2** also forms infinite chains of [Fe((mim)$_2$(mpy)COH)$_2$]$^{2+}$-cations parallel to the *c*-axis, stabilized through an n $\rightarrow$ π^*_{Ar} interaction between the MeCN solvate and the ligands' pyridine ring located on the Wyckoff position 1*h*. The distance between the centroids of the pyridine and the nitrilic nitrogen is with 3.601 Å, which is perfectly in line with the reported ranges in the literature (2.8–3.8 Å) [23], whereas the pyridine rings of the [Fe((mim)$_2$(mpy)COH)$_2$]$^{2+}$-cations on the edges of the unit cell are with distances above 4.3 Å, and are therefore out of range. Based on the mediocre stabilization of the MeCN molecules in the structure, it is hypothesized that a full solvate compound is initially formed, losing solvate molecules in time. The finite chains are stacked along the *b*-axis, the BF$_4$¯anions, and the OH-groups directed towards the next layer of [Fe((mim)$_2$(mpy)COH)$_2$]$^{2+}$ chains. It is noteworthy that, between those layers, no hydrogen bond structure is established.

The solvothermal rearrangement of the octahedral complexes results in both ligands in the formation of the [Fe$_4$O$_4$]-cubane clusters, which are chiral due to the handed arrangement of the per se achiral ligands. Cluster **3**, [Fe$_4$((mim)$_3$CO)$_4$](BF$_4$)$_4$, is highly symmetrical (Figure 4a), thus crystallizing as racemate in the cubic space group $Fd\bar{3}$ with eight [Fe$_4$O$_4$]-cores per unit cell. Four deprotonated OH-groups of the tripodal (mim)$_3$COH ligand compose with 4 Fe(II)-atoms in the distorted [Fe$_4$-(μ_3-O)$_4$]-cubane core, the surface of the cluster core decorated with the imidazole ligands. The imidazoles of each tripodal ligand coordinate to the three adjacent Fe(II)atoms next to the ligands' O-atom in the [Fe$_4$-(μ_3-O)$_4$]-cubane core. (Figure 4b) The distortion of the [Fe$_4$O$_4$]-cubane core is reflected in the Fe-O-Fe and O-Fe-O angles—77.02° for O$_1$-Fe$_1$-O$_1$ and 101.62° for Fe$_1$-O$_1$-Fe$_1$. The Fe-O bond length of 2.109 Å is about 10% longer than the Fe-O bonds reported in literature for similar iron-oxo clusters [24], which resonates well with the Fe(II) oxidation state in **3** vs. the Fe(III) oxidation state in the literature. Compared to the 1.980 Å Fe-O bond length calculated in a first principles study on Me$_4$O$_4$-cubane clusters [25], the experimentally

observed Fe-O bond is 7% longer. This suggests a slight destabilization of the Fe-O bonds, explaining the higher sensitivity of **3** towards oxygen (see Section 2.4).
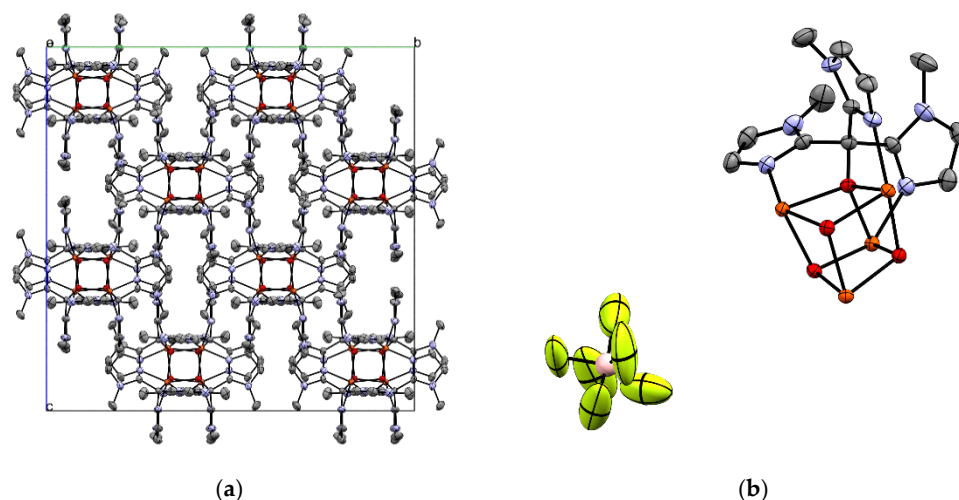

Figure 4. (**a**) Packing of $[Fe_4((mim)_3CO)_4](BF_4)_4$ (**3**), BF_4^- anions and hydrogen omitted for clarity. (**b**) Distorted $[Fe_4-(\mu_3-O)_4]$-cubane core in **3** decorated with imidazole ligands (3 ligands and hydrogen omitted for clarity). Color code: Fe orange, O red.

Based on the larger 2-methylpyridine, the $(mim)_2(mpy)COH$ ligand is less symmetrical than its $(mim)_3COH$ analogue. Whereas, in **2**, this slight asymmetry has no direct structural impact, the solvothermal rearrangement of **2** into cluster $[Fe_4(mim)_3CO)_4](BF_4)_4$ (**4**) results in a higher degree of distortion in the $[Fe_4O_4]$-cubane core, as well as in enantiomeric resolution. Moreover, **4** crystallizes the $CHCl_3$-solvate of the enantiomerically pure R-$[Fe_4((mim)_3CO)_4]$ $(BF_4)_4$ in the orthorhombic space group $P2_12_12_1$. Similar to **3**, the distorted $[Fe_4-(\mu_3-O)_4]$-cubane core builds from the deprotonated OH-groups of the tripodal $(mim)_2(mpy)COH$ ligand and the four Fe(II)-atoms (Figure 5a). Three of the four 2-methylpyridine ligands coordinate to Fe1, and the fourth 2-methylpyridine coordinates to Fe2. This asymmetric coordination also affects the bond-lengths and angles (Table 1) in the $[Fe_4O_4]$-cubane core.

Table 1. Selected bond lengths (Å) and interatomic angles (°) for **4**.

| Bond	Length (Å)	Atoms	Angle (°)	Atoms	Angle (°)
Fe1-O1	2.095(7)	O1-Fe1-O3	79.3(3)	Fe1-O1-Fe2	100.7(3)
Fe1-O3	2.096(7)	O1-Fe1-O4	78.5(3)	Fe1-O1-Fe4	100.9(3)
Fe1-O4	2.124(7)	O3-Fe1-O4	77.9(3)	Fe2-O1-Fe4	101.5(3)
Fe2-O1	2.138(7)	O1-Fe2-O2	77.7(3)	Fe2-O2-Fe3	101.1(3)
Fe2-O2	2.107(7)	O1-Fe2-O3	77.2(3)	Fe2-O2-Fe4	101.9(3)
Fe2-O3	2.150(7)	O2-Fe2-O3	77.8(3)	Fe3-O2-Fe4	100.4(3)
Fe3-O2	2.188(8)	O2-Fe3-O3	76.6(3)	Fe1-O3-Fe2	100.3(3)
Fe3-O3	2.127(7)	O2-Fe3-O4	76.4(3)	Fe1-O3-Fe3	102.3(3)
Fe3-O4	2.145(7)	O3-Fe3-O4	76.8(3)	Fe2-O3-Fe3	101.7(3)
Fe4-O1	2.134(7)	O1-Fe4-O2	76.8(3)	Fe1-O4-Fe3	100.7(3)
Fe4-O2	2.151(7)	O1-Fe4-O4	77.7(3)	Fe1-O4-Fe4	100.4(3)
Fe4-O4	2.120(7)	O2-Fe4-O4	77.8(3)	Fe3-O4-Fe4	102.8(3)
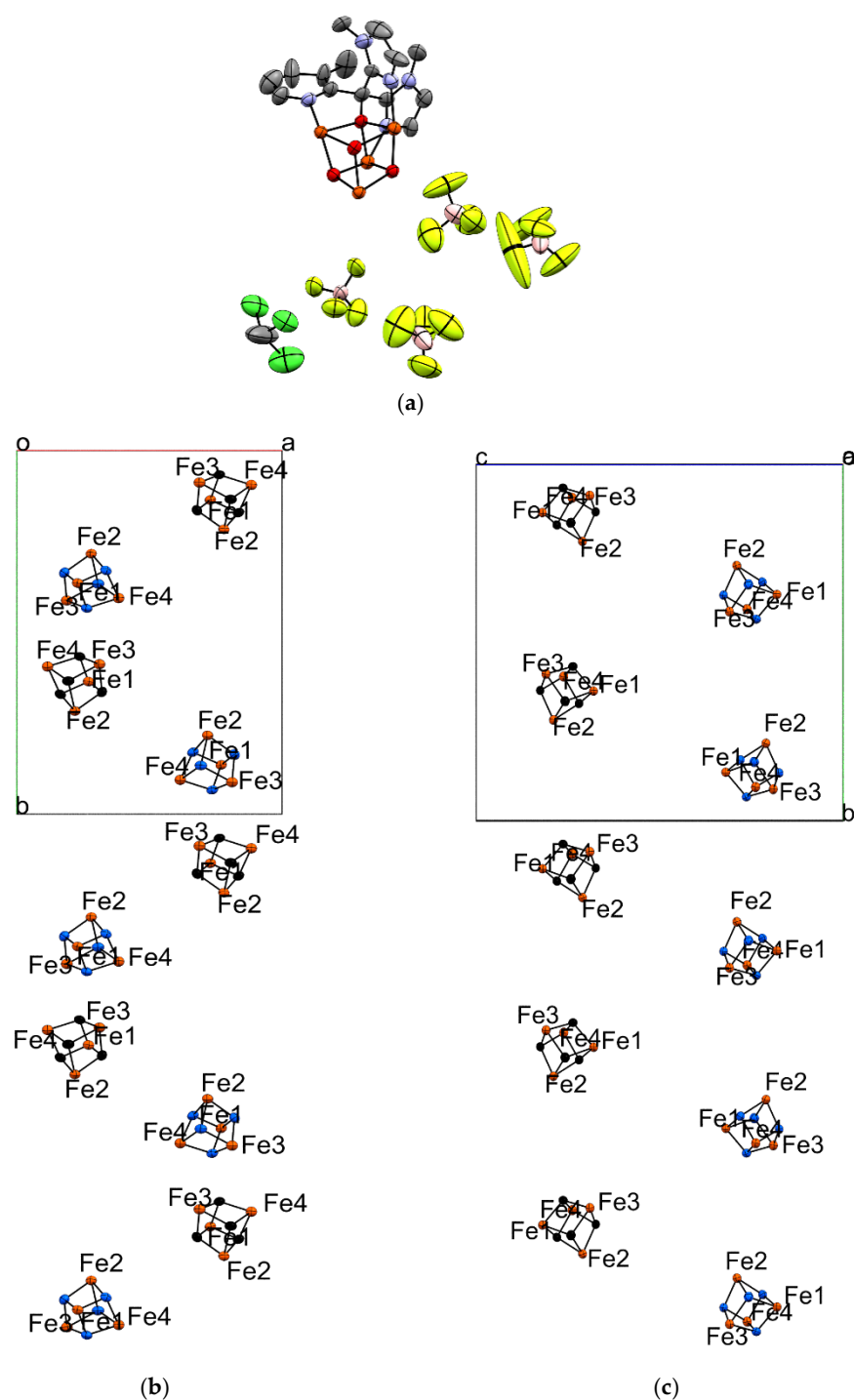
Figure 5. (**a**) Distorted [Fe_4-(μ_3-O)$_4$]-cubane core in **4** decorated with 2-methylimidazole/2-methylpyridine ligands (3 ligands and hydrogen omitted for clarity). Color code: Fe orange, O red, Cl green, F yellow, B pink. (**b**) Helical alignment of [Fe_4O_4]-cubane cores in **4** along the *b*-axis, view along *c*-axis (((mim)$_2$(mpy)CO) ligands omitted for clarity). (**c**) Location of [Fe_4O_4]-cubane cores in **4** along the *b*-axis on the 2_1 screw-axis, view along *a*-axis (((mim)$_2$(mpy)CO); ligands omitted for clarity).

Compared to **3**, the Fe-O bond lengths are slightly shorter, except for the ones involving Fe1-O1 and Fe1-O3. This is attributed to the bare 2-methylpyridine coordination environment around the Fe1 corner. Whereas, in **3**, the Fe-O-Fe and O-Fe-O angles are

all identical, in **4**, they vary between 76.4° and 79.3° for O-Fe-O and 100.3° and 102.8° for Fe-O-Fe.

Each two cluster cores form a clockwise rotating helical supramolecular alignment along the a-axis, characteristic for the R-enantiomer. (Figure 5b,c). For the refinement of the structure, a Flack parameter of 0.014(5) was obtained, which confirms the correct assignment of the given setting in the acentric space group symmetry. Moreover, it rules out any inverse setting or any related twinning of enaniomorphic forms within the investigated crystal. The molecular structure was determined in several crystal specimens from multiple crystallization batches, which all confirmed the equivalent absolute crystallographic setting, as evidenced by the absolute value and small uncertainty of the refined Flack parameter. This relates to the hypothesis, namely that cluster **4** spontaneously resolves with the identified enantiomer as its preferred form. In Table 2 the crystallographic parameters for structures 1–4 are displayed.

Table 2. Crystallographic parameters for structures **1–4**.

	1	2	3	4
Formula	$C_{15}H_{18.5}BF_4Fe_{0.5}N_7O$	$C_{16}H_{18.5}BF_4Fe_{0.5}N_{5.5}O$	$C_{52}H_{60}B_4F_{16}Fe_4N_{24}O_4$	$C_{61}H_{62}B_4Cl_3F_{16}Fe_4N_{20}O_4$
m [g mol^{-1}]	427.60	418.60	1655.88	1816.29
T [K]	200(2)	200(2)	200.15	200.15
Color	Magenta	Red	Colorless	Yellow
Shape	Block	Block	Block	Block
CrystalSystem	monoclinic	triclinic	cubic	orthorhombic
Space Group	$C2/c$	$P\bar{1}$	$Fd\bar{3}$	$P2_12_12_1$
a [Å]	16.0441(17)	11.1878(13)	24.8347(8)	16.037(3)
b [Å]	11.6518(12)	12.6938(14)	24.8347(8)	22.753(4)
c [Å]	20.049(2)	13.6370(15)	24.8347(8)	23.418(5)
α [°]	90	74.337(3)	90	90
β [°]	102.904(2)	82.058(3)	90	90
γ [°]	90	86.255(3)	90	90
V [Å^3]	3653.3(7)	1846.1(4)	15317.1(15)	8545(3)
Z	8	4	8	4
$\rho_{calc.}$ [g cm^{-3}]	1.555	1.506	1.436	1.412
μ [mm^{-1}]	0.506	0.497	0.838	0.848
Measured Refl's.	65735	51222	118123	133050
Indep't Refl's	7001	9124	1983	15661
GooF	1.016	1.017	1.106	1.026
wR_2	0.0980	0.1179	0.1969	0.1433
R_1	0.0431	0.0520	0.0636	0.0531
CCDC	2167517	2167516	2167518	2167519

2.2. Magnetic Susceptibility

Magnetic susceptibility measurements for the mononuclear complexes **1** and **2** show that both compounds remain in the iron(II) low-spin configuration over the whole measured temperature range, with values below 0.2 cm^3 K mol^{-1} and gradually decreasing as the temperature is lowered (Figure 6). The slightly faster decrease below 50 K is attributed to the zero-field splitting. The irreversible increase in susceptibility above 350 K for complex **1** (Figure 6, inset) corresponds to the partial formation of the elimination coordination compound [Fe(Me-bik)$_3$](BF$_4$)$_2$ (**5**) [20].
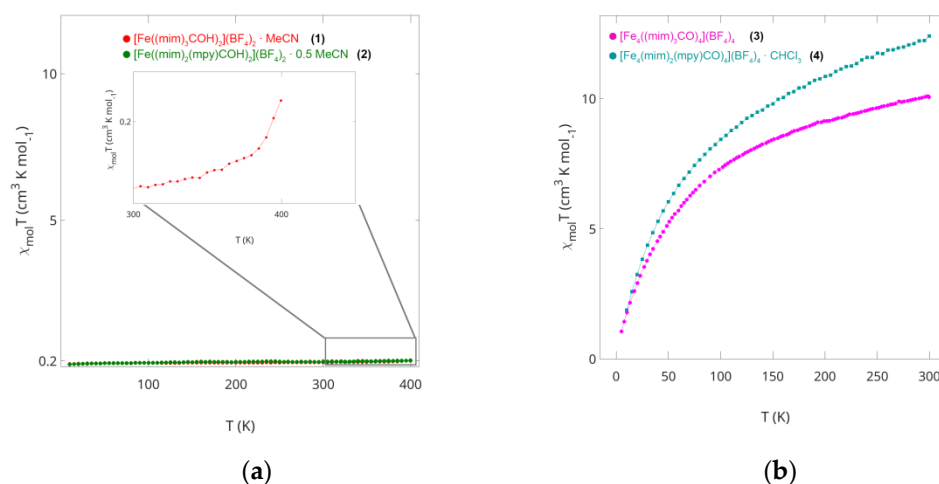
Figure 6. Temperature dependence of the magnetic susceptibility: (**a**) Mononuclear Compounds: red: Complex **1**, green: Complex **2**. (**b**) Tetranuclear Compounds: magenta: Complex **3**, cyan: Complex **4**.

The temperature dependent change of the effective magnetic moment for the $[Fe_4O_4]$ clusters **3** and **4** shows a gradual decrease from 12.4 cm^3 K mol^{-1} and 10.1 cm^3 K mol^{-1} at T = 300 K to 1.9 cm^3 K mol^{-1} and 1.8 cm^3 K mol^{-1} at T = 10 K, respectively. The value at room temperature is smaller than that of four uncoupled iron(II) atoms with a ground state of S = 8, and the gradual decrease in susceptibility upon cooling demonstrates the presence of antiferromagnetic interactions. This behavior suggests an absence of intramolecular ferromagnetic interactions, which was further substantiated by field-dependent measurement of the magnetization for a crystalline sample of **4** (Figure 7).
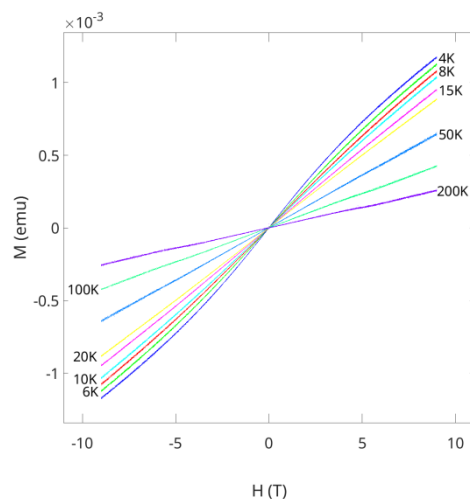

Figure 7. Field-dependent measurement of the magnetization for a crystalline sample of **4**, mounted in arbitrary orientation in the field.

2.3. ^{57}Fe-Mössbauer Spectroscopy

A ^{57}Fe-Mössbauer spectrum (Figure 8) of a microcrystalline sample of $[Fe_4O_4]$-cluster **4** shows at 4.2 K a typical Fe(II) HS-doublet, which is in good agreement with the other analyses. Fitting the spectrum provides the exclusively high spin state, without any additional magnetic phases. Because the observed doublet is the sum of four subspectra, representing the four iron sites, the electrostatic properties (isomer shift and quadrupole splitting) of the four subspectra are practically identical, because the half width of the fitted doublet is less than 50% broader than the natural line width. A separation within the given statistics is therefore not possible.
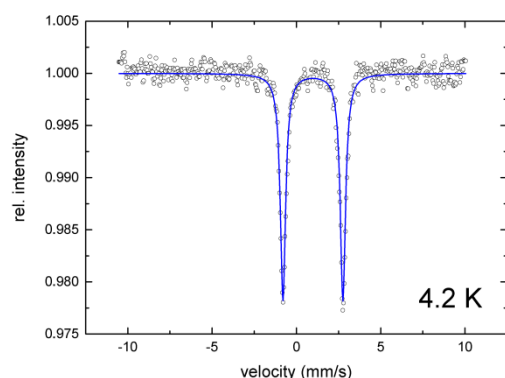
Figure 8. ^{57}Fe-Mössbauer spectrum of a microcrystalline sample of complex **4**.

2.4. Electrochemistry

A cyclic voltammogram of compounds **1** and **2** is given in Figure 9 and clearly shows the singular reversible redox-potential for the $Fe^{2+/3+}$ state at $E_{1/2}$ = 0.06 V for **1** and $E_{1/2}$ = 0.16 V for **2**. As long as an inert atmosphere is ensured, the redox cycle is fully stable. The cyclic voltammogram for the $[Fe_4O_4]$-cluster **3** shows four different redox potentials (Figure 10a), which correlate to the one-electron transitions of the four individual iron atoms each. The first three transitions describe chemically reversible processes, whereas the fourth was found to be only partially reversible.
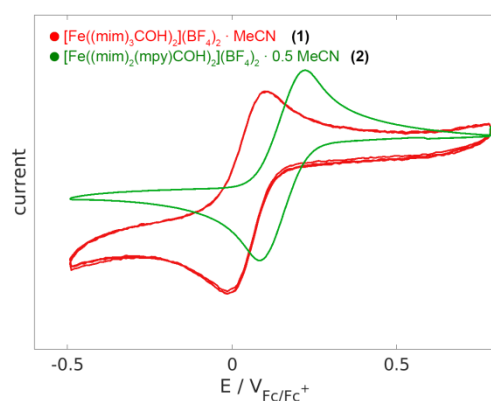

Figure 9. Cyclic voltammograms of **1** (**red**) and **2** (**green**).
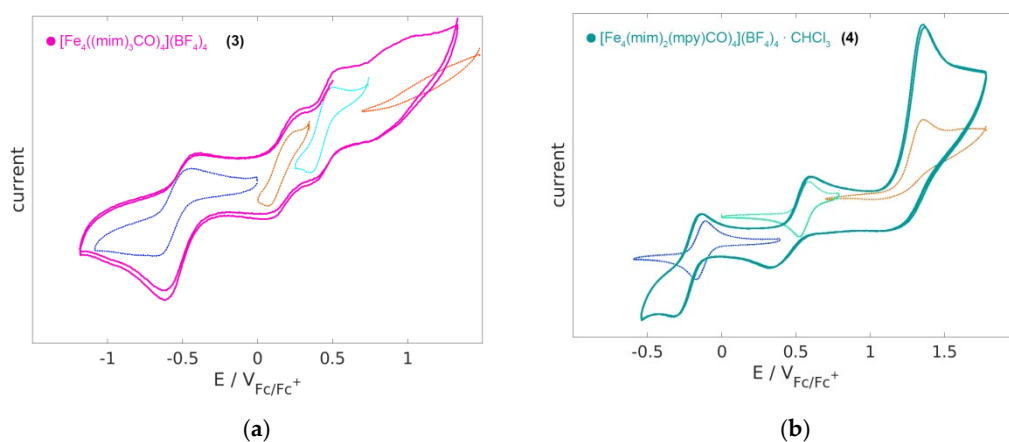

(a)

(b)

Figure 10. Cyclic voltammograms of **3** (**a**) and **4** (**b**).

The separation of anodic and cathodic peak waves of roughly 150–200 mV suggests that the electron transfer is accompanied by additional structural changes. Upon prolonged measurements, the redox behavior is gradually lost, which aligns with the quasi-

reversibility attributed to the irreversible oxidation of the $[Fe_4O_4]$-core, forming increasing amounts of Fe_3O_4. Deterioration of compound **3** in the solution is significantly increased upon contact with O_2.

In contrast, compound **4** shows extraordinary stability (Figure 10b), even in contact with air. $[Fe_4O_4]$-cluster **4** features between -0.5 V and $+2$ V three distinct and fully reversible redox waves. The first two feature one-electron oxidations, followed by a third, two-electron process. The distance between each oxidation step is greater than that for the related compound **3,** and can therefore be triggered more precisely.

Comparing the redox-potentials of **3** and **4**, the redox waves of **3** occur at ~0.5 V lower potentials than for **4**. This is in good agreement with the slightly stretched Fe-O bonds in **3** (see above), confirming their slight destabilization, and resulting in a more reactive compound.

2.5. Vibrational Spectroscopy

The investigation of the mid-infrared spectra of the mononuclear compounds **1** and **2** shows the expected bands for the heteroatomic vibrations of the imidazole and pyridine moieties in the range of 3124–3160 cm^{-1} and their carbon–carbon ring vibrations in the range of 2950–3000 cm^{-1}. The most distinct feature is the broad stretching band for their free hydroxyl groups at 3472 cm^{-1} for **1** and 3471 cm^{-1} for **2**. As the oxygen atoms become incorporated into the cube-like construct upon conversion into the clusters **3** and **4**, the OH-band completely vanishes, whereas the heterocyclic vibrations stay in the same region Figures 11 and S1).
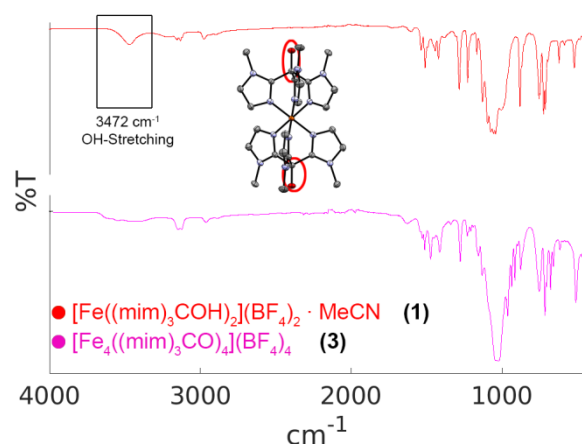

Figure 11. Comparison of the mid-range infrared spectra of **1** (**top**) and **3** (**bottom**).

3. Conclusions

The two tripodal azole ligands $((mim)_3COH)$ and $((mim)_2(mpy)COH)$ were found to form the octahedral Fe(II) low-spin complexes $[Fe((mim)_3COH)_2](BF_4)_2 \cdot MeCN$ and $[Fe((mim)_2(mpy)COH)_2](BF_4)_2 \cdot 0.5$ MeCN at room temperature. Upon heating, they reassemble reproducibly into the chiral azole-decorated distorted $[Fe_4O_4]$-cubane type clusters $[Fe_4(mim)_3CO)_4](BF_4)_4$ and $[Fe_4((mim)_3CO)_4](BF_4)_4 \cdot CHCl_3$. In the case of $[Fe((mim)_3COH)_2](BF_4)_2 \cdot MeCN$, during the solvothermal rearrangement, the octahedral $[Fe((Me-bik)_3](BF_4)_2$ is formed as a product of the elimination of an imidazole.

The octahedral Fe(II)-complexes remain in the low-spin state between 10 and 400 K. In contrast, the two $[Fe_4O_4]$-clusters are in the high-spin state (10–400 K), revealing a notable antiferromagnetic interaction. Intramolecular ferromagnetic interactions could not be observed.

Both clusters feature redox active $[Fe_4O_4]$-cubane cores with up to four individual and reversibly accessible states; however, in the case of $[Fe_4((mim)_3CO)_4](BF_4)_4$, significantly higher reactivity towards O_2 was found. The tendency for the decomposition of the $[Fe_4O_4]$-

core was found to be in alignment with the slightly elongated Fe-O bond lengths in the cluster, suggesting the reduced stabilization of the cluster core.

With this initial study on the Fe(II) coordination compounds of the tris(azole)methanol, a promising ligand system was developed, allowing for the fine-tuning of the reactivity in the octahedra and $[Fe_4O_4]$-clusters. This enables a path to a class of materials that is predetermined for the continued investigation of their redox behavior for catalytic or electron-shuttling applications.

4. Experimental Section

4.1. Methodology

If not otherwise stated, all operations involving iron(II) were carried out under inert gas atmosphere (argon 5.0). The glassware used was oven dried at 120 °C for at least 2 h before use. All solvents for the complexation reactions were dried before use and stored over 3 Å molecular sieve under argon [26]. Unless otherwise stated, all starting materials were obtained commercially and used without further purification. All NMR spectra were recorded in dry, deuterated solvents (as indicated) on a Bruker Avance UltraShield 400 MHz instrument [27]. Chemical shifts are reported in ppm; ^{1}H and ^{13}C shifts are referenced against the residual solvent resonance. The magnetic moment of the Fe(II) complexes was measured using a Physical Property Measurement System (PPMS®) by Quantum Design. The experimental setup consisted of a vibrating sample magnetometer attachment (VSM) bearing a brass sample holder with a quartz-glass powder container. The magnetic moment was determined in an external field of 1 T in the range of 10 K to 400 K, measuring at 5 K intervals with a thermal stabilization time of 5 min. The data were corrected for diamagnetic contribution. ^{57}Fe-Mössbauer measurements were performed with a standard constant acceleration spectrometer in transmission geometry. The ^{57}CoRh source was mounted on the driving system and kept at room temperature. Calibration of velocity scale was carried out with an α-Fe foil. For temperature variation between 4.2 K and room temperature a continuous flow cryostat was used in which the sample is kept in He exchange gas. Temperature stability was ±0.2 K at the measured temperatures. The spectra were analyzed by solving the full Hamiltonian with both magnetic and electrostatic interaction. Mid-range (4000–450 cm^{-1}) infrared spectra were recorded in ATR technique with a Perkin Elmer Spectrum 400, fitted with a PIKE Gladi ATR Unit [28]. Electrochemical experiments were performed with 2 mM compound and 0.1 M NBu$_4$BF$_4$ in acetonitrile using a Pt-plate-working and auxiliary electrode, measured versus the Fc/Fc$^+$ couple with a usual scan rate of 100 mVs^{-1} at room temperature using an Agilent 33120A Waveform Generator and an Agilent 34970A Data Acquisition Unit. Single crystals were attached to a glass fiber by using perfluorinated oil and were mounted on a Bruker KAPPA APEX II diffractometer equipped with a CCD detector with Mo Kα radiation (Incoatec Microfocus Source IμS: 30 W, multilayer mirror, λ = 0.71073 Å). For all measurements, data were reduced to intensity values by using SAINT Plus, and an absorption correction was applied by using the multi scan method implemented by SADABS [29]. For structure solutions by direct methods and the structure refinements, the programs SHELXT [30] and SHELXL-2018/3 [31] were used, respectively. All non H-atoms were refined with anisotropic displacement parameters. The residual electron densities corresponding to disordered solvent residues in **4** were flattened by the SQUEEZE algorithm of PLATON [32].

4.2. Synthesis

tris(1-methyl-*1H*-imidazol-2-yl)methanol *((mim)$_3$COH)*

The title compound was prepared based on the synthesis of Sorrell and Borovik with slight modifications [33]. To a solution of 1-methyl-imidazole (20.47 g, 249.3 mmol), in anhydrous THF (300 mL), n-butyl-lithium was slowly added (as 2.5 M solution in hexane, 100 mL, 250 mmol). Upon complete addition, the dark orange solution was cooled to −78 °C, and a cooled solution of methyl chloroformate (7.28 g, 77.0 mmol) in THF (30 mL) was added dropwise. The mixture was allowed to slowly warm to room temperature

overnight. The reaction was quenched by the addition of acetic acid and all volatiles were evaporated under reduced pressure. The residue was extracted with dichloromethane, dried over MgSO$_4$, and recrystallized from acetone to yield the title compound as pale-yellow crystals (15.48 g, 74%).

^{1}H NMR (400 MHz, CDCl$_3$) δ = 6.90 (d, J = 1.2 Hz, 3H), 6.84 (d, J = 1.2 Hz, 3H), 5.94 (s, 1H), 3.36 (s, 9H).

^{13}C NMR (101 MHz, CDCl3) δ = 146.05, 126.42, 123.71, 71.43, 34.07.

IR (cm^{-1}): 3453, 3152, 3121, 2968, 1537, 1508, 1419, 1284, 1227, 1168, 1129

bis(1-methyl-*1H*-imidazol-2-yl)(3-methylpyridin-2-yl)methanol *((mim)$_2$(mpy)COH)*

To an ice-cold solution of 1-methyl-imidazole (6 g, 73.1 mmol), in anhydrous THF (300 mL), n-buthyl-lithium was slowly added (as 2.5 m solution in hexane, 30 mL, 74.9 mmol). Upon the complete addition, the solution was stirred for 40 min and was afterwards further cooled to −90 °C. A cooled solution of methyl 3-methylpicolinate (5.52 g, 36.5 mmol) in anhydrous THF (60 mL) was slowly added. The reaction was slowly allowed to warm up to room temperature and stirred overnight. The reaction was quenched by the addition of 150 mL saturated and aqueous NH$_4$Cl. Most of the organic solvent was evaporated under reduced pressure, and the residue was extracted three times with chloroform, washed once with water and brine, and afterwards dried with MgSO$_4$. All volatiles were evaporated under reduced pressure to yield an oily residue, which was further purified by recrystallization from benzene to yield the title compound as a colorless solid (7.07 g, 68.3%).

^{1}H NMR (400 MHz, CDCl$_3$) δ = 8.35 (ddd, J = 4.8, 1.6, 0.7 Hz, 1H), 7.48 (ddd, J = 7.6, 1.5, 0.7 Hz, 1H), 7.44 (s, 1H), 7.19 (dd, J = 7.5, 4.8 Hz, 1H), 6.85 (d, J = 1.2 Hz, 2H), 6.80 (d, J = 1.2 Hz, 2H), 3.38 (s, 6H), 1.77 (s, 3H).

^{13}C NMR (101 MHz, CDCl$_3$) δ = 155.85, 146.90, 143.70, 140.71, 134.47, 129.05, 128.24, 126.58, 125.31, 123.73, 123.01, 73.86, 34.38, 18.67.

[Fe((mim)$_3$COH)$_2$](BF$_4$)$_2$ · MeCN (1)

Two equivalents of ligand (mim)$_3$COH (100 mg, 0.36 mmol) were added to a colorless solution of Fe(BF$_4$)$_2$ · 6 H$_2$O (62 mg, 0.18 mmol) in acetonitrile and were stirred for 3 h at room temperature, resulting in a pink solution. The solvent was evaporated under reduced pressure, and the pink residue was washed two times with diethyl ether to obtain the mononuclear complex as magenta solid (141 mg, 94.9%). Magenta block-shaped single crystals were obtained by slow diffusion of diethyl ether into a saturated acetonitrile solution of **1** overnight.

[Fe((mim)$_2$(mpy)COH)$_2$](BF$_4$)$_2$ · 0.5MeCN (2)

Using the same synthetic procedure as for compound **1**, the title compound was obtained as red solid (136 mg, 97.3%). Red block-shaped single crystals were obtained by slow diffusion of diethyl ether into a saturated acetonitrile solution of **2** overnight.

[Fe$_4$((mim)$_3$CO)$_4$](BF$_4$)$_4$ (3)

A glass microwave vial was charged with a solution of Fe(BF$_4$)$_2$·6 H$_2$O (62 mg, 0.18 mmol) in ethanol and an equimolar methanolic solution of ligand (mim)$_3$COH (50 mg, 0.18 mmol). Immediately, a pinkish precipitate formed, and the reaction was stirred for 5 min at room temperature and was afterwards heated rapidly to 140 °C. A slow transition from a pinkish precipitate to a grey dispersion was observed. The reaction was stopped after heating for 30 min and before the change of the reaction color to blue by immediately cooling below room temperature. The precipitate was separated by centrifuge and washed twice with ethanol (4 mL). Evaporation of solvent traces under high vacuum yielded the title compound as a grey solid (46 mg, 15.1%). Colorless single crystals were obtained by slow diffusion of diethyl ether into an acetonitrile solution of **3** after approximately one week.

[Fe$_4$((mim)$_2$(mpy)CO)$_4$](BF$_4$)$_4$ · CHCl$_3$ (4)

A glass microwave vial was charged with a solution of Fe(BF$_4$)$_2$·6 H$_2$O (62 mg, 0.18 mmol) in ethanol and an equimolar methanolic solution of ligand (mim)$_2$(mpy)COH (52 mg, 0.18 mmol). Immediately, a red precipitate formed, and the reaction was stirred for 5 min at room temperature and was afterwards heated rapidly to 140 °C. The reaction was

kept at this temperature overnight, upon which a yellow precipitate slowly formed. The product was separated by centrifuge and washed once with ethanol (4 mL) and chloroform (4 mL). Evaporation of solvent traces under high vacuum yielded the title compound as a yellow solid (67 mg, 21.5%). Crystals were obtained by slow vapor diffusion of $CHCl_3$ to an acetonitrile solution of **4** over a few days.

[Fe(Me-bik)$_3$](BF$_4$)$_2$ (5)

Two equivalents of ligand $(mim)_3COH$ (100 mg, 0.36 mmol) were added to a colorless solution of $Fe(BF_4)_2 \cdot 6\ H_2O$ (62 mg, 0.18 mmol) in acetonitrile and were stirred at 60 °C overnight, upon which the pink reaction mixture had turned dark blue. The solution was evaporated to yield a dark blue residue, which was subsequently washed with diethyl ether to obtain the title compound as a dark solid (37 mg, 38%). Dark colored singe crystals were obtained by the solvothermal crystallization of an acetonitrile/dichloromethane (1:1) solution of **5** in a sealed glass vial at 60 °C over several days.

Supplementary Materials: The following supporting information can be downloaded at: https://www.mdpi.com/article/10.3390/magnetochemistry8090095/s1, Figure S1: Mid-range infrared spectrum of 2 and 4; Figure S2: ^{1}H NMR of tris(1-methyl-1H-imidazol-2-yl)methanol; Figure S3: ^{13}C NMR of tris(1-methyl-1H-imidazol-2-yl)methanol; Figure S4: ^{1}H NMR of bis(1-methyl-1H-imidazol-2-yl)(3-methylpyridin-2-yl)methanol; Figure S5: ^{13}C NMR of bis(1-methyl-1H-imidazol-2-yl)(3-methylpyridin-2-yl)methanol.

References

1. Quesada, M.; Kooijman, H.; Gamez, P.; Costa, J.S.; van Koningsbruggen, P.J.; Weinberger, P.; Reissner, M.; Spek, A.L.; Haasnoot, J.G.; Reedijk, J. [Fe (μ-btzmp) 2 (btzmp) 2](ClO 4) 2: A doubly-bridged 1D spin-transition bistetrazole-based polymer showing thermal hysteresis behaviour. *Dalton Trans.* **2007**, *46*, 5434–5440. [CrossRef] [PubMed]

2. Koudriavtsev, A.B.; Stassen, A.F.; Haasnoot, J.G.; Grunert, M.; Weinberger, P.; Linert, W. Theoretical description of phenomena observed in a systematic study of the spin crossover in Fe (ii) complexes with halogenated ethyltetrazoles Part II. The quasi-chemical model (specific molecular interactions). *Phys. Chem. Chem. Phys.* **2003**, *5*, 3676–3683. [CrossRef]

3. Halcrow, M.A. Iron (II) complexes of 2, 6-di (pyrazol-1-yl) pyridines—A versatile system for spin-crossover research. *Coord. Chem. Rev.* **2009**, *253*, 2493–2514. [CrossRef]

4. Tang, C.C.; Davalian, D.; Huang, P.; Breslow, R. Models for Metal Binding Sites in Zinc Enzymes. Syntheses of tris [4 (5)-Imidazolyl] carbinol (4-TIC), tris (2-Imidazolyl) carbinol (2-TIC), and Related Ligands, and studies on metal complex binding constants and spectra. *J. Am. Chem. Soc.* **1978**, *100*, 3918–3922. [CrossRef]

5. Brown, R.S.; Huguet, J. Synthesis and physical studies of pyridine and imidazole containing tridentate metal binding ligands. *Can. J. Chem.* **1980**, *58*, 889–901. [CrossRef]

6. Wu, L.P.; Yamagiwa, Y.; Ino, I.; Sugimoto, K.; Kuroda-Sowa, T.; Kamikawa, T.; Munakata, M. Unique tetranuclear copper (II) cluster and monomeric iron (II),(III) complexes with a tris (imidazolyl) chelating ligand. *Polyhedron* **1999**, *18*, 2047–2053. [CrossRef]

7. Baran, P.; Boca, R.; Chakraborty, I.; Giapintzakis, J.; Herchel, R.; Huang, Q.; McGrady, J.E.; Raptis, R.G.; Sanakis, Y.; Simopoulos, A. Synthesis, characterization, and study of octanuclear iron-oxo clusters containing a redox-active Fe4O4-cubane core. *Inorg. Chem.* **2008**, *47*, 645–655. [CrossRef]

8. Shoner, S.C.; Power, P.P. Neutral catecholate derivatives of manganese and iron: Synthesis and characterization of the metal-oxygen cubane-like species M4 (DBCat) 4 (py) 6 (M = Mn, Fe), the trinuclear complex Mn3 (DBCat) 4 (py) 4, and the dimers M2 (DBCat) 2 (py) n (M = Mn, n = 6; M = Fe, n = 4, 6). *Inorg. Chem.* **1992**, *31*, 1001.

9.   Taft, K.L.; Caneschi, A.; Pence, L.E.; Delfs, C.D.; Papaefthymiou, G.C.; Lippard, S.J.J. Iron and manganese alkoxide cubes. *Am. Chem. Soc.* **1993**, *115*, 11753. [CrossRef]

10.   Taft, L.; Papaefthymiou, G.C.; Lippard, S.J. A mixed-valent polyiron oxo complex that models the biomineralization of the ferritin core. *Science* **1993**, *259*, 1302. [CrossRef]

11.   Taft, K.L.; Papaefthymiou, G.C.; Lippard, S.J. Synthesis, structure, and electronic properties of a mixed-valent dodecairon oxo complex, a model for the biomineralization of ferritin. *Inorg. Chem.* **1994**, *33*, 1510. [CrossRef]

12.   Dell'Amico, D.B.; Boschi, D.; Calderazo, F.; Ianelli, S.; Labella, L.; Marchetti, F.; Pelizzi, G.; Quadrelli, E.G.F. N, N-Dialkylcarbamato μ-oxo derivatives of iron (III). *Inorg. Chim. Acta* **2000**, *300–302*, 882.

13.   Oshio, H.; Hoshino, N.; Ito, T.J. Superparamagnetic behavior in an alkoxo-bridged iron (II) cube. *Am. Chem. Soc.* **2000**, *122*, 12602. [CrossRef]

14.   Oshio, H.; Hoshino, N.; Ito, T.; Nakano, M.J. Single-molecule magnets of ferrous cubes: Structurally controlled magnetic anisotropy. *Am. Chem. Soc.* **2004**, *126*, 8805. [CrossRef] [PubMed]

15.   Lee, D.; Sorace, L.; Caneschi, A.; Lippard, S.J. Hydroxo-bridged cubane-type tetrairon (II) clusters supported by sterically-hindered carboxylate ligands. *Inorg. Chem.* **2001**, *40*, 6774. [CrossRef]

16.   Clemente-Juan, J.M.; Mackiewicz, C.; Verelst, M.; Dahan, F.; Bousseksou, A.; Sanakis, Y.; Tuchagues, J.-P. Synthesis, structure, and magnetic properties of tetranuclear cubane-like and chain-like iron (II) complexes based on the N4O pentadentate dinucleating ligand 1, 5-bis [(2-pyridylmethyl) amino] pentan-3-ol. *Inorg. Chem.* **2002**, *41*, 1478. [CrossRef]

17.   Abrahams, B.F.; Hudson, T.A.; Robson, R.J. Highly symmetric networks derived from cubane-related octametallic complexes of a new oxyanion of carbon, C4O74-, each molecule attached to eight neighbors by 24 equivalent hydrogen bonds. *Am. Chem. Soc.* **2004**, *126*, 8624. [CrossRef]

18.   Hudson, T.A.; Berry, K.J.; Moubaraki, B.; Murray, K.; Robson, R. Citrate, in Collaboration with a Guanidinium Ion, as a Generator of Cubane-like Complexes with a Range of Metal Cations: Synthesis, Structures, and Magnetic Properties of [C (NH2) 3] 8 [(MII) 4 (cit) 4]⊙ 8H2O (M = Mg, Mn, Fe, Co, Ni, and Zn; cit = Citrate). *Inorg. Chem.* **2006**, *45*, 3549. [CrossRef]

19.   Gass, I.A.; Milios, C.J.; Whittaker, A.G.; Fabiani, F.P.A.; Parsons, S.; Murrie, M.; Perlepes, S.P.; Brechin, E.K. A cube in a tetrahedron: Microwave-assisted synthesis of an octametallic FeIII cluster. *Inorg. Chem.* **2006**, *45*, 5281. [CrossRef]

20.   De, S.; Tewary, S.; Garnier, D.; Li, Y.; Gontard, G.; Lisnard, L.; Flambard, A.; Breher, F.; Boillot, M.L.; Rajaraman, G.; et al. Solution and Solid-State Study of the Spin-Crossover [FeII (R-bik) 3](BF4) 2 Complexes (R = Me, Et, Vinyl). *Eur. J. Inorg. Chem.* **2018**, *2018*, 414–428. [CrossRef]

21.   Drew, M.G.B.; Harding, C.J.; McKee, V.; Morgan, G.G.; Nelson, J. Geometric Control of Manganese Redox State. *J. Chem. Soc. Chem. Commun.* **1995**, 1035–1038. [CrossRef]

22.   Alvarez, S.; Alemany, P.; Casanova, D.; Cirera, J.; Llunell, M.; Avnir, D. Shape maps and polyhedral interconversion paths intransition metal chemistry. *Coord. Chem. Rev.* **2005**, *249*, 1693–1708. [CrossRef]

23.   Bartlett, G.J.; Newberry, R.W.; VanVeller, B.; Raines, R.T.; Woolfson, D.N. Interplay of hydrogen bonds and n→π* interactions in proteins. *J. Am. Chem. Soc.* **2013**, *135*, 18682–18688. [CrossRef]

24.   Raptis, R.G.; Georgakaki, I.P.; Hockless, D.C. A FeIII/oxo cubane contained in an octanuclear complex of T symmetry that is stable over five oxidation states. *Angew. Chem. Int. Ed.* **1999**, *38*, 1632–1634. [CrossRef]

25.   Datta, S.; Rahaman, B. First principles study of electronic structure for cubane-like and ring-shaped structures of M4O4, M4S4 clusters (M= Mn, Fe, Co, Ni, Cu). *AIP Adv.* **2015**, *5*, 117231. [CrossRef]

26.   Armarego, W.L. *Purification of Laboratory Chemicals*; Butterworth-Heinemann: Amsterdam, The Netherlands; Elsevier Inc.: Amsterdam, The Netherlands, 2013. [CrossRef]

27.   Bruker Analytical X-ray Instruments, I. Available online: https://www.bruker.com/products (accessed on 22 July 2022).

28.   Müller, D.; Knoll, C.; Seifried, M.; Weinberger, P. ATR or transmission—A variable temperature study comparing both techniques using [Fe (3ditz) 3](BF4) 2 as model system. *Vib. Spectrosc.* **2016**, *86*, 198–205. [CrossRef]

29.   Bruker, I. Bruker AXS Inc.: Madison, WI, USA, 2012. Available online: https://www.bruker.com/products (accessed on 22 July 2022).

30.   Sheldrick, G.M. SHELXT—Integrated space-group and crystal-structure determination. *Acta Crystallogr. Sect. A Found. Adv.* **2015**, *71*, 3–8. [CrossRef]

31.   Sheldrick, G.M. Crystal structure refinement with *SHELXL. Acta Cryst. C* **2015**, *71*, 3–8. [CrossRef]

32.   Spek, A.L. PLATON SQUEEZE: A tool for the calculation of the disordered solvent contribution to the calculated structure factors. *Acta Crystallogr. Sect. C Struct. Chem.* **2015**, *71*, 9–18. [CrossRef]

33.   Sorrell, T.N.; Borovik, A.S. Synthesis, structure, and spectroscopic properties of an unusual copper (I) dimer having imidazole ligands. A model for the carbonyl derivative of hemocyanin and implications for the structure of deoxyhemocyanin. *J. Am. Chem. Soc.* **1987**, *109*, 4255–4260. [CrossRef]